

Submitted to the Astrophysical Journal (Letters)

**The Hard-X-ray to Gamma-ray Spectrum
in the EGRET AGNs**

Marco Fatuzzo[†] and Fulvio Melia^{*1}

[†]Physics Department, The University of Arizona, Tucson, AZ 85721

^{*}Physics Department and Steward Observatory, The University of Arizona, Tucson, AZ 85721

Received _____; accepted _____

¹Presidential Young Investigator.

ABSTRACT

EGRET (20 MeV to 30 GeV) on board the *Compton* GRO has observed high-energy emission from about $\sim 40 - 50$ Active Galactic Nuclei. Theoretical models of this emission based on the upscattering of thermal disk photons by cooling, relativistic electrons can successfully account for the EGRET observations, but they predict a considerably greater X-ray flux than that actually observed in a majority of these sources. This inconsistency may be an indication that the particles are energized during the Compton scattering process, since the X-ray emission is produced by the lowest energy electrons, whose density may be relatively small due to the acceleration. Such a situation may arise as a result of resistive field generation in electromagnetic acceleration schemes, which we here explore. A key feature of this model is the assumed existence of a current associated with the azimuthal component B_ϕ of the underlying magnetic field by a slight imbalance in the energy distributions of outwardly moving, relativistic electrons and protons produced at the disk surface via shock acceleration. The generation of an electric field (via magnetic field line reconnection) is thus required to maintain the current in the presence of a resistivity induced by the radiative drag on the relativistic electrons. We show that the resulting spectrum can exhibit a significant deficit of X-rays compared with γ -rays. In addition, due to the uni-directional flow of the current associated with B_ϕ , this model would predict that the electrons are energized relative to the protons in the outflow only on one side of the disk. They should be decelerated on the reverse side. As such, we would anticipate that any given blazar should have a $\sim 50\%$ probability of being γ -bright, which appears to be consistent with the observed ratio.

Subject headings: acceleration of particles — accretion disks — black hole physics — galaxies: Active — magnetic fields — radiative transfer

1. Introduction

Many active galactic nuclei (AGNs) produce radio jets or strong radio core emission whose origin is still not completely understood. Because many quasars are also luminous X-ray sources whose strength is correlated with the radio core emission (Browne & Murphy 1987), it is believed that understanding the high-energy emission, which probably originates close to the central, supermassive black hole, will yield important insights into the formation of these jets and the radio emission mechanism. During the past few years, EGRET on the Compton GRO (designed to measure photon energies from 20 MeV to 30 GeV) has detected about 50 AGNs, of which ~ 40 are high confidence detections (Mukherjee et al. 1997). Most of them are quasars, at least six are BL Lac objects, and at least 13 are Optically Violent Variables. The vast majority are radio loud, flat spectrum objects ranging from a redshift z of 0.03 to more than 2.0. Typical blazar (i.e., AGNs whose dominant observational characteristics appear to be due to beaming effects) spectra suggest the presence of a break below ~ 10 MeV if the γ -ray component is to connect smoothly with the observed X-ray spectrum at lower energies. This gamma-ray emission is most likely associated with a particle acceleration region near the black hole, thereby providing tantalizing clues into the physical processes acting in this environment.

A wide variety of particle energizing mechanisms have been proposed for the jet formation, ranging from radiation pressure-driven flows (Abramowicz & Piran 1980) to electromagnetically-driven self-similar jets (Li, Chiueh & Begelman 1992). The most enduring models are the electromagnetic ones because they alone appear to have the capability of accelerating particles to the relativistic speeds necessary to account for the radiative characteristics of superluminal sources. The retardation of the particles due to the photon Comptonization in the intense radiation field of these compact regions has been recognized ever since it was discovered that high-velocity jets could be decelerated by

particle-photon collisions. This mechanism is sometimes used to account for the low terminal Lorentz factors ($\gamma_\infty \lesssim 10$) observed in superluminal sources (Phinney 1982). Subsequently, Melia & Königl (1989) demonstrated that the Compton deceleration due to scatterings with accretion disk photons could transfer most of the jet’s mechanical energy into an observable flux of high-energy radiation, accounting for both the low values of γ_∞ and the relatively flat X-ray spectra seen in some sources. Indeed, inverse Compton scattering models involving a cooling population of leptons have been successful in reproducing many of the EGRET observations. However, the incomplete cooling of these leptons in the presence of the disk’s nonuniform photon field results in spectral breaks between the γ -ray and X-ray regimes of ~ 0.5 (Dermer & Schlickeiser 1993), a result that does not account for the large variety of spectral breaks seen in the EGRET AGNs (von Montigny et al. 1995a). While the presence of additional energy-loss mechanisms can increase the spectral break to ~ 0.7 (Dermer, Sturmer & Schlickeiser 1997), it seems that the underlying problem with standard cooling models is the relative overabundance of low-energy electrons in the assumed power-law distributions. To this end, recent theoretical efforts invoking Comptonization have assumed the presence of an electron acceleration process to shift all of the leptons to high energy, thereby producing a low-energy cutoff in the electron distribution. This energizing is assumed to occur either before injection into the emission region (e.g., Böttcher, Mause & Schlickeiser 1997; Dermer, Sturmer & Schlickeiser 1997; Sikora et al. 1997) or throughout the interaction zone (Marcowith, Henri & Pelletier 1995; Bednarek, Kirk & Mastichiadis 1996). While these models have had success in accounting for both the X-ray and γ -ray data, the physics of how these conditions arise remains unsettled, particularly with regard to the specifics of the acceleration scheme in the latter class of models.

In this paper, we will be addressing two principal issues. First, we attempt to develop a physically self-consistent picture for the mechanism that produces the required particle distribution with a low-energy cutoff. Second, we will follow the evolution of the particle

properties with distance away from the source of injection, and we will determine the effect of this on the cumulative photon spectrum. The view studied here is that low-energy electrons are first energized in a thin transition region in order to produce the current associated with the presence of a curled magnetic field and they then continue to be accelerated *during* the Comptonization process in order to maintain this current. Unlike previous models of this type, the acceleration scheme is well-specified and the electron distribution is determined self-consistently. The overall process is assumed to occur within an approximately force-free magnetosphere, as first described by Blandford & Znajek (1977). Following Melia & Königl (1989), we assume the presence of a luminous accretion disk (often invoked to account for the observed “blue” bump) whose radiation scatters with the accelerating particles. The magnetosphere thus retains a small resistivity due to the particle-photon interactions that couple the acceleration of the particles and their concurrent radiative emission, but the fields remain close to their force-free intensities. This resistivity induces a component of the electric field parallel to the underlying magnetic field that drives the outflow. The object of our model is to determine the individual particle dynamics and the upscattered radiation spectrum self-consistently. The merit of such an approach is evident, in that the energized photon distribution depends critically on the particle energies. In §2, we describe a scenario with which the magnetospheric current may be produced, and we discuss how this current would be a source of γ -ray emission. Our calculations and results are presented in §3, where we also discuss their relevance to the observations.

2. The Particle Dynamics and High-Energy Emission

For simplicity, the disk is taken to be a geometrically flat, blackbody emitter with inner radius R_{in} , outer radius R_{out} and a radius-dependent surface temperature as given by

(Pringle 1981)

$$T(R) = T_{max} \left\{ 7 \left(\frac{49 R_{in}}{36 R} \right)^3 \left[1 - \left(\frac{R_{in}}{R} \right)^{1/2} \right] \right\}^{1/4}, \quad (1)$$

where the maximum temperature $T_{max} \equiv (3GM_*\dot{M}/56\pi\sigma_B R_{max}^3)^{1/4}$ (where M_* is the black hole mass, \dot{M} is the rate of mass transfer through the disk and σ_B is the Stefan-Boltzmann constant) is attained at the (equatorial) radius $R_{max} = (49/36)R_{in}$. The system is naturally described by a cylindrical coordinate system with an origin centered at the black hole and with the \hat{z} direction normal to the disk. In this first set of simulations, the magnetic field B threading the disk is assumed to be axisymmetric and, as a result of disk rotation, to have an azimuthal component B_ϕ .

The gravitational energy dissipation power is characterized by $\dot{E}_{accr} \equiv GM_*\dot{M}/R_{in}$. About half of this energy is dissipated throughout the disk. In the picture developed here, we assume that energy is transferred to a sub-population of electrons and protons via shock acceleration at a rate $\eta\dot{E}_{accr}$ throughout an active region that extends from the inner edge of the disk out to a radius $R_a \ll R_{out}$ (η characterizing the efficiency of the particle energizing process). Using the above expressions for T_{max} and R_{max} , the rate at which the particles gain mechanical energy is expressed as

$$\dot{E}_{mech} = 4.2 \times 10^{41} \text{ ergs s}^{-1} \left(\frac{\eta}{0.1} \right) \left(\frac{T_{max}}{5 \times 10^4 \text{ K}} \right)^4 \left(\frac{M_*}{10^7 M_\odot} \right)^2 \left(\frac{R_{in}}{3R_g} \right)^2, \quad (2)$$

where $R_g = 2GM_*/c^2$ is the Schwarzschild radius.

As a result of shock acceleration, the energized protons are expected to acquire a relativistic energy distribution characterized by a power-law in the Lorentz factor γ . While the electrons are also expected to acquire a relativistic energy distribution, the details of this process are not well understood. As such, we make the reasonable assumption that the energized electrons are also characterized by a power-law distribution in γ but we do not require that the spectral indices for the two populations be equal. In principle, a

complex magnetic field structure would impose a complicated angular distribution for the charges. We note, however, that the observation of GeV photons in the EGRET spectrum, coupled with high UV/X-ray luminosities and rapid variability, drastically constrain the beam “size” of the high-energy emission (e.g., von Montigny et al. 1995a). This in turn limits the range of possible magnetic field geometries (i.e., $B_\phi \ll B$), and suggests that the dynamics of the outflowing particles may be approximated by a more or less unidirectional motion. (The resulting γ -ray emission does, however, depend on the angular distribution of the electrons. This point will be addressed below.) For simplicity, we further assume here that $B_r = 0$ and take the energized particles to move directly outward along the \hat{z} direction (since $B_\phi \ll B$). For a uniform active region, the initial relativistic electron (proton) distribution function is therefore $n_{e(p)}(\gamma; z = 0, r) = C \gamma^{-\alpha_{e(p)}}$ for $1 < \gamma < \gamma_{u;e(p)}$, where $n_{e(p)}(\gamma; z, r) d\gamma$ is the number density of electrons (protons) at (r, z, ϕ) with a Lorentz factor between γ and $\gamma + d\gamma$. Note that since $m_p \gg m_e$, almost all of the mechanical energy is carried by the protons for comparable values of spectral indices. For simplicity, we assume throughout this paper that $\alpha_p = 2.5$. The results of our calculations will therefore be insensitive to the value of the upper bound for the proton distribution $\gamma_{u;p}$. The value of the upper bound $\gamma_{u;e}$ for the electron distribution is determined by balancing the rate of acceleration within the shock region with the combined rate of cooling due to synchrotron and Compton processes (Begelman, Rudak & Sikora 1990). It is important to note that synchrotron cooling dominates over Compton cooling within the shock region since the magnetic field is expected to be highly disordered within that region (thereby resulting in large pitch angles between the local magnetic field direction and the electron motion) and the magnetic energy density is appreciably greater than the photon energy density. This therefore leads to a maximum Lorentz factor $\gamma_u = 1.16 \times 10^6 (B/10^4 G)^{-1/2}$. For simplicity, we adopt the fiducial value $\gamma_u = 10^6$ in our simulations. In contrast, since the magnetic field becomes ordered away from the disk and the electron motion becomes nearly parallel

to the field direction, Compton cooling processes dominate the dynamics of the flow above the disk. For a uniform active region, the value of the number density of energized particles is found by equating (2) with the expression for the mechanical energy flux carried by the protons $\dot{E}_p \approx \langle \gamma_p \rangle m_p c^2 2\pi R_a^2 c n_{e0}$, where $\langle \gamma_p \rangle$ is the average Lorentz factor for the protons, m_p is the proton rest mass, and the factor of 2 takes into account both sides of the disk. Assuming that the flow is charge neutral, the number density of electrons energized by the shocks can therefore be expressed as

$$n_{e0} \approx 6.2 \times 10^4 \text{ cm}^{-3} \left(\frac{\langle \gamma_p \rangle}{3} \right)^{-1} \left(\frac{\eta}{0.1} \right) \left(\frac{T_{max}}{5 \times 10^4 \text{ K}} \right)^4 \left(\frac{R_a}{10 R_{in}} \right)^{-2}. \quad (3)$$

(We note that for the assumed power-law index $\alpha_p = 2.5$ for the proton distribution, $\langle \gamma_p \rangle = 3$ so long as $\gamma_{u;p} \gg 1$.)

The shock mechanism which energizes the electrons and protons acts independently of the large scale magnetic field structure through which the outflowing particles then move. We therefore assume that the particles must undergo an adjustment in their distribution within a (presumably narrow) transition layer in order to produce the current associated with the presence of B_ϕ . We do not attempt to develop a complete account of this process here but rather postulate that it occurs within a height z_0 due to the action of an electric field generated by magnetic field line reconnection so as to attain a self-consistent magneto-dynamic system. This assumption is reasonable as long as the particle energy density $u \approx \dot{E}_{mech}/\pi R_a^2 c$ is much smaller than $u_B \equiv B^2/8\pi$, thereby constraining the radius of the active region to a value $R_a \gg (8\dot{E}_{mech}/B^2 c)^{1/2}$. A comparison between n_{e0} in Equation (3) and the critical number density necessary to produce the required current

$$n_c \equiv \frac{J}{ec} \sim \frac{B_\phi}{4\pi e R_\phi} = 0.56 \text{ cm}^{-3} \left(\frac{B_\phi}{10^4 \text{ G}} \right) \left(\frac{R_\phi}{R_g} \right)^{-1} \left(\frac{M_*}{10^7 M_\odot} \right)^{-1} \quad (4)$$

(where R_ϕ is the characteristic radius of curvature of B_ϕ), then suggests that n_c is probably due to a slight imbalance between the electron and proton velocity distributions since

$n_c \ll n_{e0}$. Throughout the transition zone, the electron distribution undergoes either an upward or downward shift, depending on the direction of B_ϕ . Since the electric field shifts all the electrons over a given distance by the same $\Delta\gamma$ (ignoring pile-up effects at $\gamma = 1$ for a downward shift; these electrons do not contribute to the γ -ray emission), the electron power-law distribution is maintained throughout the transition zone but the value of the lower cut-off γ_l may be raised. As such, we shall assume a power-law for $n_e(\gamma; z_0, r)$ at the transition zone boundary and take γ_l to be a free parameter characterizing the dynamical processes occurring during the transition. The shift in γ_u is small enough for us to ignore as long as $\gamma_{l,e} \ll 10^6$. Furthermore, as long as $\gamma_{l,e} \ll m_p/m_e$, the corresponding shift in the proton distribution can also be ignored. To summarize, it appears that both the negative and positive charges maintain their outward relativistic motion, but on balance the electrons are either slightly faster or slightly slower than the protons in order to account for the required current n_c to maintain B_ϕ . As we shall see, these two situations result in significantly different γ -ray emissivities, and this difference may therefore constitute an important observational signature.

In the absence of any resistive forces, the electric field would be quenched once the required current is produced by the time the particles reach z_0 . However, cooling processes (primarily from inverse Compton scatterings with the disk photons) above z_0 continue to downshift the energy distribution of the electrons and protons (Melia & Königl 1989). As such, this “Compton resistance” results in the generation of an electric field to maintain the current throughout the entire emission region. (We assume that the relativistic proton distribution does not change due to Compton upscatterings since by comparison with the electrons, the proton Compton scattering cross section, and hence the proton resistivity, is significantly smaller.) To determine the effect of these interactions on the electron distribution, we first calculate the response of a single electron at (z, r, ϕ) moving with Lorentz factor γ through the radiation field in the \hat{z} direction.

Primed quantities denote values in the electron rest frame, whereas unprimed parameters pertain to the disk frame (hereafter referred to as the lab frame). The radiation field above the disk is characterized by the specific photon number density per solid angle $n_{ph}(\varepsilon, T[R]) = (2\varepsilon^2/h^3c^3)(\exp\{\varepsilon/kT[R]\} - 1)^{-1}$, where ε is the lab-frame photon energy and $T[R]$ is the radius-dependent temperature. The electron moving through this field scatters dN photons to energies between ε_s and $\varepsilon_s + d\varepsilon_s$ and solid angles between $\mu_s\phi_s$ and $[\mu_s + d\mu_s][\phi_s + d\phi_s]$ at a rate (per energy per solid angle)

$$\frac{dN}{dt d\varepsilon_s d\mu_s d\phi_s} = \int_{ph} d\varepsilon \int_{disk} \left[\frac{\mu R dR d\Phi}{d^2} \right] n_{ph}(\varepsilon, T[R]) \left(\frac{d\sigma_{KN}}{d\mu'_s d\phi'_s d\varepsilon'_s} \right) \frac{c(1 - \beta\mu)}{\gamma(1 - \beta\mu_s)}, \quad (5)$$

where $\beta = (1 - \gamma^{-2})^{-1/2}$, $d \equiv (z^2 + [r \cos(\phi) - R \cos(\Phi)]^2 + [r \sin(\phi) - R \sin(\Phi)]^2)^{1/2}$ is the distance between the electron and disk element $R dR d\Phi$ located at (R, Φ) , and $\mu = z/d$ is the cosine of the angle between the direction of the scattered photons originating from the disk at (R, Φ) and the electron's direction of motion. (Note that μ is also the cosine of the angle between the direction of the photons incident on the electron and the direction normal to the disk.) The expression in square brackets represents the solid angle subtended by the disk element $R dR d\Phi$ at (R, Φ) with respect to the electron. The differential Klein-Nishina cross-section $d\sigma_{KN}/d\mu'_s d\phi'_s d\varepsilon'_s$ is evaluated in the electron rest frame. Using the general expressions relating the lab and rest frame energies ($\varepsilon' = \varepsilon\gamma[1 - \beta\mu]$) and angles ($\mu' = [\mu - \beta]/[1 - \beta\mu]$; $\phi' = \phi$), one finds the relation $d\varepsilon_s d\mu_s d\phi_s/d\varepsilon'_s d\mu'_s d\phi'_s = \gamma(1 - \beta\mu_s)$, thereby allowing Equation (4) to be easily integrated over all scattered photon energies and solid angles to yield the single electron scattering rate. From this follows the γ -dependent mean-free path length for the electron:

$$l_{mfp}(\gamma; z, r) \equiv \left[\frac{dN(\gamma; z, r)}{c dt} \right]^{-1} = \left[\int_{ph} d\varepsilon \int_{disk} \left[\frac{\mu R dR d\Phi}{d^2} \right] n_{ph}(\varepsilon, T[R]) \sigma_{KN}(\varepsilon') (1 - \beta\mu) \right]^{-1}. \quad (6)$$

As a result of a single scattering with a photon of energy ε and direction μ , an electron

with initial Lorentz factor γ attains a lower Lorentz factor γ_s in accordance with the energy conservation equation $\gamma_s = \gamma - [\varepsilon\gamma^2(1 - \beta\mu)]/[m_e c^2 + \varepsilon\gamma(1 - \beta\mu)]$, where for computational ease, we have set μ'_s and $\bar{\mu}'$ to their average values (i.e., $\mu'_s = \bar{\mu}' = 0$). Thus, scattering that occurs within a distance dz reduces the number density of electrons with Lorentz factors between γ and $\gamma + d\gamma$ by $n_e(\gamma; z, r)d\gamma dz/l_{mfp}(\gamma; z, r)$. Since the particle number is conserved, this decrease corresponds to an increase in the number density of electrons with a Lorentz factor between γ_s and $\gamma_s + d\gamma_s$ of $n_e(\gamma; z, r)d\gamma_s dz/l_{mfp}(\gamma; z, r)$. In the absence of a restoring force (i.e., if there were no electric field), the average value of the Lorentz factor $\langle\gamma\rangle$ would undergo a gradual downward shift. As mentioned above, however, this downward shift in the electron density function must be balanced by the presence of an electric field which maintains the average Lorentz factor $\langle\gamma\rangle$ of the distribution, in order to sustain the current associated with B_ϕ . Since the electric field shifts all electrons moving through the same distance by the same $\Delta\gamma$, we first calculate the change in the electron distribution function as a result of scattering along a path element dz and then linearly shift the degraded distribution function upward so as to maintain the value of $\langle\gamma\rangle$. Repeating this procedure stepwise moving outward from z_0 provides a determination of $n_e(\gamma; z, r)$ for all z .

With the electron distribution thus specified, the γ -ray Compton emissivity can be determined by integrating Equation (4) over the entire scattering electron population. However, while a unidirectional motion was assumed above, the sensitivity of the photon production rate to the angle between the electron direction of motion and the scattered photon direction requires a more realistic treatment of the electron angular distribution. We leave the details of this development to future work. The fact that a strong correlation is observed between γ -ray emissivity and blazar activity suggests that γ -rays are emitted within a relatively narrow cone (see, e.g., von Montigny et al. 1995a). We here assume that this cone has an opening angle $\theta_c \sim 5^\circ$, and average the overall photon production rate over

$1 \geq \mu_s \geq \cos 5^\circ$. Thus, the rate at which photons are detected by an observer at a distance D (ignoring redshift effects) is given by the expression

$$\frac{dN_{obs}}{dt d\varepsilon_s dA} = \frac{2\pi}{(1 - \cos 5^\circ) D^2} \int_{z_0}^{\infty} dz \int_{R_{in}}^{R_a} r dr \int_1^{\infty} d\gamma \int_{\cos 5^\circ}^1 d\mu_s n_e(\gamma; z, r) \frac{dN}{dt d\varepsilon_s d\mu_s d\phi_s}, \quad (7)$$

where azimuthal symmetry has been invoked to perform the integral over ϕ and average over ϕ_s and the relationship between the scattered photon solid angle $d\mu_s d\phi_s$ and the detector area dA (i.e., $dA = D^2 d\mu_s d\phi_s$) has been used.

3. Results and Discussion

(a) Particle Distributions and Characteristic Spectra

In this section, we present the results of a calculation for a $10^7 M_\odot$ black hole surrounded by a disk with $T_{max} = 5 \times 10^4$ K and inner and outer radii $R_{in} = 3R_g$ and $R_{out} = 500R_g$ (where in this case $R_g \approx 3 \times 10^{12}$ cm). Although the luminosity associated with this system ($L \approx 2 \times 10^{42}$ ergs s^{-1}) corresponds to the weakest observed AGNs, qualitatively similar results are expected to follow from the modeling of more powerful sources, though this will require substantially more extensive computational resources. The active “shock” region is assumed to extend out to a radius $R_a = 10 R_{in}$, and the distance to the source is set to 100 Mpc. The efficiency η is taken to be 10% and the transition zone boundary z_0 is placed at an arbitrary value of $5R_g$. The dependence of our results on the actual value of z_0 is weaker than their dependence on the other unknowns in the problem, such as $\gamma_{l;e}$, as long as $z_0 \ll R_{out}$. We have therefore chosen to concentrate our simulations on a parameter search corresponding to the dominant variables. We note, however, that the radiation field from the disk is anisotropic, and a careful treatment of the transition layer may produce some differences with the results shown here.

Before discussing these results, let us first analyze the photon spectrum produced by a power-law electron distribution with spectral index α injected at z_0 that completely cools via inverse-Compton scattering with the disk photons (i.e., the well-studied scenario in which there is no re-energizing, e.g., due to an electric field). The resulting radiation spectrum is characterized by a power-law ($dN_{ph} \propto \varepsilon_s^{-\Gamma}$) with index $\Gamma = (\alpha + 2)/2$ for energies above the characteristic value $\varepsilon_{ch} \equiv 3kT_{max}$ ($\approx 10^{-5}$ MeV for the parameter space considered here). In practice, however, only electrons with γ greater than a critical value γ_c (≈ 100 for these conditions) cool appreciably (see, e.g., Dermer & Schlickeiser 1993; von Montigny et al. 1995a; and references cited therein). As such, the distribution function of the outwardly moving electrons will evolve until it exhibits a break at $\sim \gamma_c$. The corresponding photon spectrum, in turn, will exhibit a break at energy $\sim \gamma_c^2 \varepsilon_{ch}$ ($\approx 10^{-1}$ MeV), below which the spectral index will be $\Gamma = (\alpha + 1)/2$. This effect produces a broken power-law spectrum with a shift in Γ between the X-rays and γ -rays of $\Delta\Gamma \approx 0.5$ (see cooling spectra for $\gamma_l = 1$ in figures [3a] and [3b]; hereafter, γ_l always refers to the electrons).

This situation changes considerably in the presence of an electric field that acts above the transition zone to maintain the value of $\langle\gamma\rangle$ for the electron distribution injected at z_0 . In order to offset the energy lost by the high-energy electrons (which cool very efficiently via their interactions with the radiation field), an electric field is established that shifts all of the electrons upward, including the low-energy part of the distribution. The electrons thus “bunch” up at $\langle\gamma\rangle$, which in turn produces a bump in the photon spectrum at an energy $\langle\gamma\rangle^2 \varepsilon_{ch}$. The overall spectral shape of the upscattered photons depends on how the value of $\langle\gamma\rangle$ compares with γ_c . This point is illustrated in Figures 1 and 2. Figure 1a shows the evolution of the electron distribution function at ten different values of z for the model parameters $\alpha = 2$ and $\gamma_l = 1$. The curves in figure 1a correspond to the values $(z - z_0)/R_g = 0.0027, 0.011, 0.030, 0.080, 0.21, 0.53, 1.4, 3.5, 9.1,$ and 23 , with the lowest value corresponding to the power-law curve and the subsequent values pertaining to the

curves evolving away from this initial distribution. The value of $\langle\gamma\rangle$ for this evolution is 13.8. As expected, the low-energy electrons are shifted upward and bunch near $\langle\gamma\rangle$ while the high-energy electrons cool to γ_c . The resulting photon spectrum is shown in Figure 2. Since $\langle\gamma\rangle < \gamma_c$, the bump at $\langle\gamma\rangle^2 \varepsilon_{ch}$ ($\approx 10^{-3}$ MeV) is succeeded by a curve that softens to a power-law with spectral index $\Gamma \approx 2$ for energies greater than $\gamma_c^2 \varepsilon_{ch}$ (0.1 MeV). The resulting shift in spectral index (i.e., ≈ 0.5) between the X-ray and γ -ray parts of the spectrum is similar to that found in the absence of an electric field.

In contrast to the previous case where $\gamma_l = 1$, Figure 1b shows the evolution of the electron distribution function for ten different values of z when $\alpha = 2$ and $\gamma_l = 100$. The curves in figure 1b correspond to the values $(z - z_0)/R_g = 0.0033, 0.013, 0.033, 0.090, 0.23, 0.58, 1.5, 3.7, 9.3,$ and 23, with the lowest value corresponding to the power-law curve and the subsequent values pertaining to the curves evolving away from this initial distribution. In this case, $\langle\gamma\rangle \approx 920$. The greater value of $\langle\gamma\rangle$ over γ_c results in all electrons bunching near $\langle\gamma\rangle$. The resulting photon spectrum is shown in Figure 2. Since $\langle\gamma\rangle > \gamma_c$, the bump at $\langle\gamma\rangle^2 \varepsilon_{ch}$ (≈ 10 MeV) is succeeded by a power-law with spectral index $\Gamma \approx 2$. This spectrum is not well represented by a broken power-law. We note here that the energized distribution ($\gamma_l = 100$) is injected with approximately 70 times the energy of the $\gamma_l = 1$ distribution and as such produces ≈ 70 times more high energy photons. This point will be elaborated upon later in the discussion.

(b) Comparison with the Data

The high energy photon spectra (30 MeV to 30 GeV) of AGNs observed by EGRET are well-represented by a power-law with a spectral index ranging from 1.4 to 3.0. This spectrum is a natural consequence of the inverse Compton scattering of thermal disk photons by a cooling power-law distribution of relativistic electrons, though this would seem to require a range in the electron distribution index α between 0.8 and 4.0 which may

be broader than that produced by shock acceleration. As we have discussed above, the problem with this scenario arises from the fact that a purely cooling electron distribution with $\gamma_l = 1$ produces a spectrum that is not consistent with many AGN X-ray observations in that it predicts a larger emission of X-rays than is observed (von Montigny et al. 1995a). In contrast, it is clear from Figures 1 and 2 that a low energy cut-off in the electron energy distribution function, together with an electric field that maintains the average Lorentz factor of the outflowing electrons in the presence of inverse-Compton scattering with the disk radiation, can significantly reduce the predicted UV and X-ray spectral components. To illustrate this point in the context of the observations, we present in Figure 3a the flux density spectra for the model parameters $\alpha = 2$ and $\gamma_l = 1, 10,$ and 100 , along with the multiwavelength data from PKS 0827+243 and in Figure 3b the flux density spectra for the model parameters $\alpha = 3$ and $\gamma_l = 1, 10,$ and 100 , along with the multiwavelength data from PKS 1741-038 (taken from Figure 5 of von Montigny et al. 1995a). The dotted lines extending from the three different spectra on each figure are for cooling populations with corresponding values of γ_l at the transition zone. The different scales were chosen for easy comparison of the data (represented by the left hand scale) to the model results (represented by the right hand scale). We have not attempted to optimize the fit here, so the difference between the observed and calculated fluxes is presumably due to an imprecise choice of the black hole mass M , source distance D , and choice of γ_l .

It is evident from our results that the presence of an energizing region which shifts the electron population upward is sufficient to produce a spectrum devoid of X-rays. The subsequent acceleration does, however, produce an observable signature in the form of a bump around 10 MeV. As one can see from Figure 3, the main effect of this feature on the high-energy component of the spectrum is a turn-up toward lower γ -ray energies. There may in fact already be some evidence of this in several of the EGRET AGNs discussed by von Montigny et al. (1995a).

(c) Gamma-ray Faint Versus Gamma-ray Loud Sources

A second important prediction of this model is that because the current associated with B_ϕ is due to an imbalance between the proton and electron outflow rates, the sign of the charge flux should be opposite on either side of the disk. So the electrons are re-energized in the transition zone on one side, but the Lorentz factor of their counterparts on the reverse side must be down-shifted. Since the apparent luminosity is sensitive to the value of γ_l , AGNs observed from the energized side of the disk are clearly much more likely to have a high (or observable) γ -ray flux, compared with those observed from the backside. The expectation is that only about half of the superluminal radio sources should therefore be observable in γ -rays, with a possible additional correlation between the spectral break and distance.

In their analysis of superluminal and strong flat-spectrum radio quasars that were not seen by EGRET, von Montigny et al. (1995b) showed that about 35 sources that would otherwise be expected to be strong γ -ray emitters were γ -quiet, compared to roughly 40 – 50 that were detected (either strongly or marginally). The lack of evidence for any definitive characteristics distinguishing these two groups led them to suggest two primary reasons for the difference: 1) time variability, and 2) orientation and beam geometry effects. The scenario we have developed in this paper would point to a third reason, namely that the undetected sources are for the most part γ -quiet due to the uni-directional current flow associated with B_ϕ . As we have discussed above, the electrons are somewhat decelerated relative to the protons on one side of the disk, rendering them ineffective in Compton upscattering the ambient low-energy radiation.

However, since the observed radio emission associated with the superluminal motion is produced many parsecs away from the central engine, we would not expect in this model to see a correlation between γ -faintness and a lack of longer-wavelength blazar activity. Since

most of the mechanical energy flux is carried by the protons, the energy budget available for broadband emission in the more extended outflow is roughly equal on both sides of the disk. So the B_ϕ -induced current flow may offer an elegant explanation for the distinction between γ -loud and γ -faint blazars.

Finally, on a related matter, one may argue using the curves in Figure 3 that the X-rays may also be produced by the same mechanism that accounts for the γ -radiation, if the X-ray portion of the spectrum rises as indicated by the theoretical curves in this waveband. Note that to fit both the γ -ray and X-ray data, we would need $\gamma_l \approx 50$ for PKS 0827+243 and $\gamma_l \approx 100$ for PKS 1741-038. Unfortunately, the available data are not yet sufficient for us to distinguish between this situation and one in which the X-rays constitute a completely separate component. Future observations may identify the X-ray spectral index with the required precision for us resolve this issue.

Acknowledgments

This work was partially supported by NASA grant NAG 5-3075. We are very grateful to the anonymous referee for his very helpful comments. We also thank E. Marietta for helpful discussions during the early stages of this work.

4. Figure Captions

Fig. 1a - Evolution of the electron distribution function for ten different values of z when $\alpha = 2$ and $\gamma_l = 1$. The curves correspond to $(z - z_0)/R_g = 0.0027, 0.011, 0.030, 0.080, 0.21, 0.53, 1.4, 3.5, 9.1,$ and 23, with the lowest value indicating the initial power-law and subsequent values pertaining to the curves evolving away from this. The units on the vertical scale are arbitrary.

Fig. 1b - Evolution of the electron distribution function for ten different values of z when $\alpha = 2$ and $\gamma_l = 100$. The curves correspond to $(z - z_0)/R_g = 0.0033, 0.013, 0.033, 0.090, 0.23, 0.58, 1.5, 3.7, 9.3,$ and 23, with the lowest value indicating the initial power-law and subsequent values pertaining to the curves evolving away from this.

Fig. 2 - The photon spectrum as seen by an observer at a distance of 100 Mpc for $\alpha = 2$ and the two indicated values of γ_l . These spectra are associated with the particle distributions depicted in Fig. 1.

Fig. 3 - (a) Flux density spectrum as seen by an observer at a distance of 100 Mpc for $\alpha = 2$ and the three indicated values of γ_l (right-hand scale). Multiwavelength observations of PKS 0827+243 are included for comparison (left hand scale). The data are taken from von Montigny et al. (1995a). (b) The flux density spectrum as seen by an observer at a distance of 100 Mpc for $\alpha = 3$ and the three indicated values of γ_l (right-hand scale). Multiwavelength observations of PKS 1741-038 are included for comparison (left hand scale). The data are taken from von Montigny et al. (1995a).

REFERENCES

- Abramowicz, M. A. & Piran, T. 1980, *ApJ*, **241**, L7.
- Antonucci, R., & Barvainis, R. 1988, *ApJ*, **332**, L13.
- Bednarek, W., Kirk, J. G. & Mastichiadis A. 1996, *A&A*, 120, 571
- Begelman, M. C., Rudak, B. & Sikora, M. 1990, *ApJ*, **362**, 38.
- Blandford, R. D. & Znajek, R. L., 1977, *MNRAS*, **179**, 433.
- Böttcher, M., Mause, H. & Schlickeiser, R., 1997, *A&A*, 324, 395
- Browne, I. W. A. & Murphy, D. W. 1987, *MNRAS*, **226**, 601.
- Dermer, C. D., & Schlickeiser, R. 1993, *ApJ*, **416**, 458.
- Dermer, C. D., Sturmer, S. J. & Schlickeiser, R. 1997, *ApJS*, 109, 103
- Li, Z., Chiueh, T. & Begelman, M. C. 1992, *ApJ*, **394**, 459.
- Marcowith, A., Henri, G. & Pelletier, G. 1995, *MNRAS*, **277**, 681.
- Melia, F. & Königl, A. 1989, *ApJ*, **340**, 162.
- Mukherjee, R., et al. 1997, *ApJ*, **490**, 116.
- Phinney, E. S. 1982, *MNRAS*, **198**, 1109.
- Pringle, J. E. 1981, *ARA&A*, 19, 137
- Sikora M. et al. 1997, *ApJ*, **484**, 108.
- von Montigny, C. et al 1995a, *ApJ*, **440**, 525.

von Montigny, C. et al 1995b, A&A, 299, 680

Figure 1a

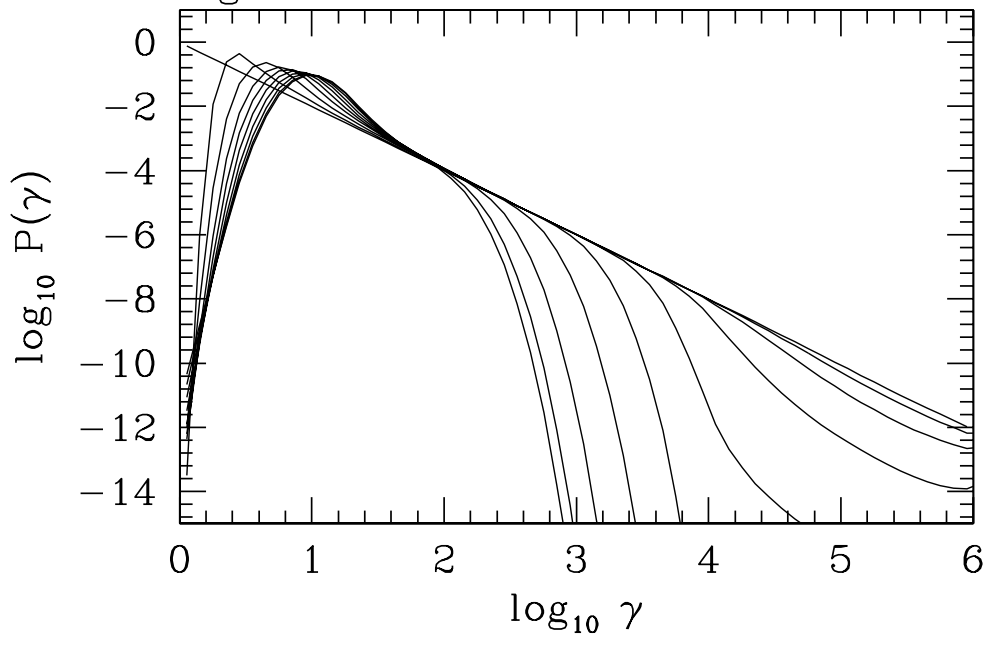


Figure 1b

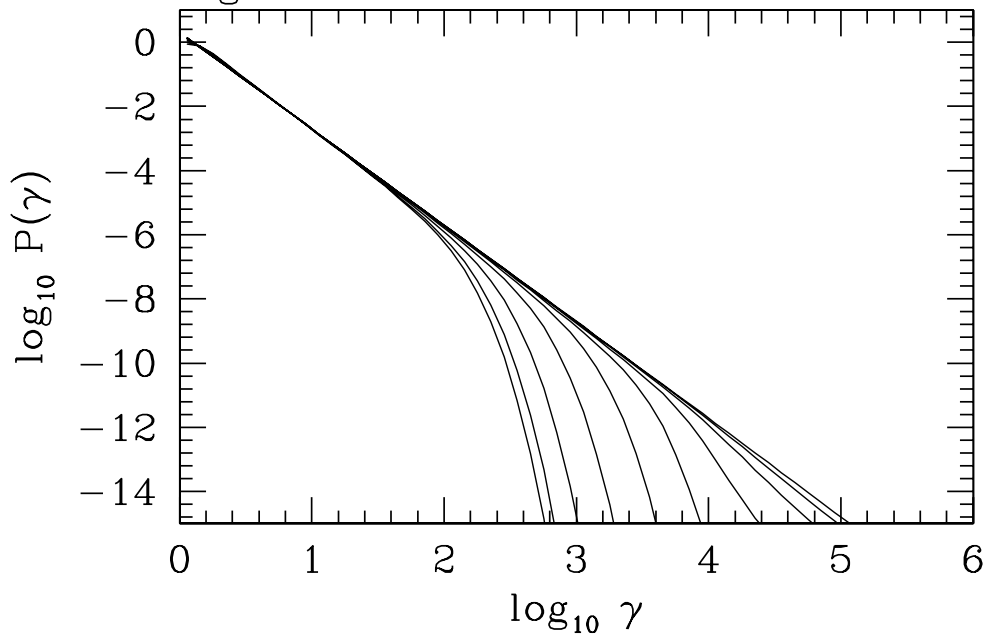


Figure 2

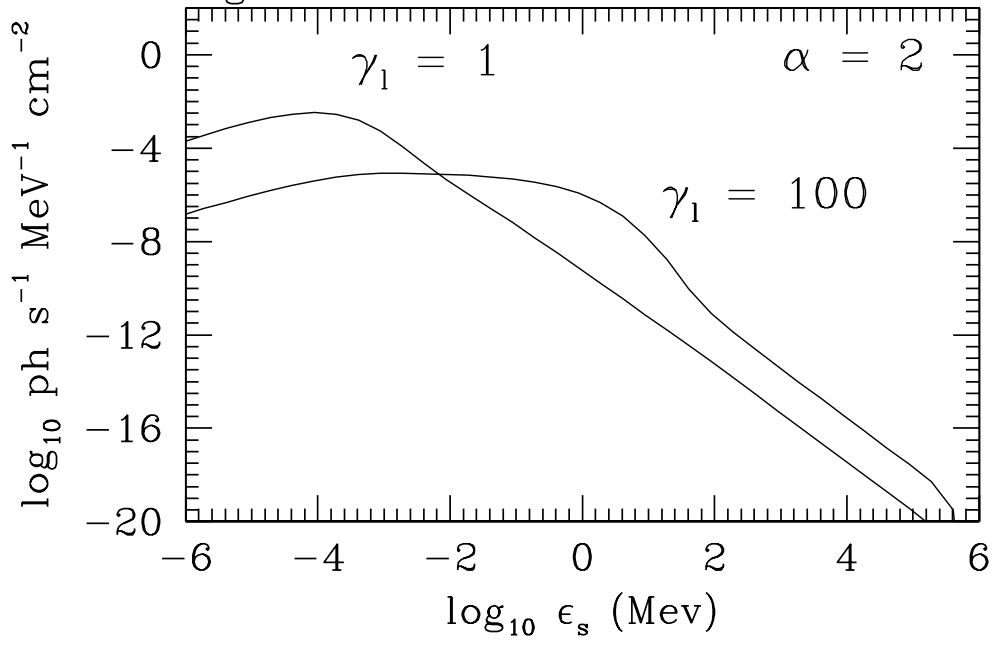


Figure 3

